Facultad de Física
Grado en Física
curso 2020-21
Trabajo Fin de Grado

Photometric observations of eclipsing binary star systems

Author:
D. Galán Diéguez

Tutor:
J.P. Garzón Heydt
Física Atómica, Molecular y Nuclear, Departamento de Física de Partículas.
Universidade de Santiago de Compostela

Cotutor:
R. Iglesias Marzoa
Grupo de Operaciones Telescópicas, Centro de Estudios de Física del Cosmos de Aragón

June 2021

Facultad de Física
Grado en Física
curso 2020-21
Trabajo Fin de Grado

Photometric observations of eclipsing binary star systems

Author: **Daniel Galán Diéguez**

Tutor: **Juan Pablo Garzón Heydt**,
LabCAF/ IGFAE (Instituto Gallego de Fisica de Altas Energias), Física Atómica, Molecular y Nuclear, Departamento de Física de Partículas. Universidade de Santiago de Compostela.
juanantonio.garzon@usc.es

Cotutor: **Ramón Iglesias Marzoa**,
Grupo de Operaciones Telescópicas, Centro de Estudios de Física del Cosmos de Aragón
riglesias@cefca.es

I cannot express enough thanks to my tutors for their support and encouragement: Juan Pablo Garzón Heydt, who has allowed me to do this TFG and Ramón Iglesias Marzoa, who has discovered the fantastic world of binary star systems for me. I would also like to make a special mention to María Jesús Arévalo, who has allowed me to make the observations at the Observatorio del Teide, trusting me to carry them out alone. I cannot forget Basilio Ruiz Cobo, that if astrophysics has become one of my passions is thanks to the way he transmits them in his classes.

Getting here could not have been accomplished without the support of my family and friends: thank you for your faith and support over the past four years in the university, without your advice and affection I would not have reached where I am.

Date of presentation: June 2021

Declaration signed by the author of the originality of the work

The author of the work declares that this is an original work. At the same time, he authorizes the control by personnel of the Universidade de Santiago de Compostela of said originality, eventually through the use of databases and their inclusion in them.

In Santiago de Compostela, on June 28, 2021.

Sgd. Daniel Galán Diéguez

Author's authorization to disseminate the work

The author authorizes the dissemination of the work for the purposes considered in the current regulations of the TFG and TFM of the Universidade de Santiago de Compostela (Artigo 11.3) and the TFM of the Máster en Física (Artigo 33), understanding that this authorization does not influence the intellectual property of the work or the possibility of publishing it totally or partially by other means. At the same time, he authorizes that the Facultad de Física of that University have an electronic copy of the work for its filing, consultation and use for academic and research uses with the specific mention of the author.

In Santiago de Compostela, on June 28, 2021.

Sgd. Daniel Galán Diéguez

Abstract

Throughout this work, the procedure carried out to do photometric observations of two eclipsing binary star systems, 2MASS J01074282+4845188 and ASAS J052919-1617.3, will be explained.

First, the design and preparation of the different remote observation nights, using the CAMELOT2 camera of the IAC80 telescope of the Observatorio del Teide (Tenerife), will be detailed. In this process, key elements in the observation of these objects will be determined: observation times, filters to be used, exposure times and eclipse instants through the ephemeris equation. Using the CCD images obtained, their reduction will be carried out, through the `IRAF` software, using the bias and flat-field images, which will allow their correction and trimming. Then, in order to establish a relationship between pixel position and equatorial coordinates, images astrometry is performed; thus, binary systems and comparison stars can be located from their celestial coordinates.

Using an adaptive aperture photometry, which allows to configure it according to seeing conditions, the instrumental magnitudes of the binary systems and their comparison stars will be obtained, which will allow differential photometry to be carried out. After this, different computational techniques will make possible to obtain the primary eclipses instants during the observation nights; in this way, the periods of the different binary systems will be calculated through the ephemeris equation. Finally, using the results of the origin of the ephemeris and the period, the eclipsing binary star systems light curves will be obtained.

Resumen

A lo largo de este trabajo se explicará el procedimiento llevado a cabo para la realización de observaciones fotométricas de dos sistemas binarios eclipsantes: 2MASS J01074282+4845188 y ASAS J052919-1617.3.

En primer lugar se detallará el diseño y preparación de las diferentes noches de observación remota empleando la cámara CAMELOT2 del telescopio IAC80 del Observatorio del Teide (Tenerife). En este proceso se determinarán elementos clave en la observación de estos objetos: momentos de observación, filtros a emplear, tiempos de exposición y los instantes de eclipses a través de la ecuación de efemérides. Usando las imágenes CCD obtenidas, se llevará a cabo su reducción, a través del software `IRAF`, empleando las imágenes bias y flat-field, que permitirán su corrección y recorte. A continuación, con el objetivo de establecer una relación entre posición de los píxeles y coordenadas ecuatoriales, se realiza la astrometría de las imágenes, pudiendo así localizar los sistemas binarios y estrellas de comparación a partir de sus coordenadas celestes.

Empleando una fotometría de apertura adaptativa, que permite configurarla de acuerdo a las condiciones de seeing, se obtendrán las magnitudes instrumentales de los sistemas binarios y sus estrellas de comparación, que permitirán llevar a cabo la fotometría diferencial. Tras esto, diferentes técnicas de computación posibilitarán la obtención de los instantes de los eclipses primarios durante las noches de observación; de esta manera, se lograrán calcular los periodos de los diferentes sistemas binarios a través de la ecuación de efemérides. Finalmente, empleando los resultados de instante de inicio de las efemérides y el periodo, se obtendrán las curvas de luz de los sistemas binarios eclipsantes.

Resumo

Ao longo deste traballo explicarase o procedemento levado a cabo para a realización de observacións fotométricas de dous sistemas binarios eclipsantes: 2MASS J01074282+4845188 e ASAS J052919-1617.3.

En primeiro lugar detallarase o deseño e preparación das diferentes noites de observación remota empregando a cámara CAMELOT2 do telescopio IAC80 do Observatorio del Teide (Tenerife). Neste proceso determinaranse elementos chave na observación destes obxectos: momentos de observación, filtros a empregar, tempos de exposición e os instantes de eclipses a través da ecuación de efemérides. Usando as imaxes CCD obtidas, levarase a cabo a súa redución, a través do software `IRAF`, empregando as imaxes bias e flat-field, que permitirán a súa corrección e recorte. A continuación, co obxectivo de establecer unha relación entre posición dos píxeles e coordenadas ecuatoriais, realízase a astrometría das imaxes, podendo así localizar os sistemas binarios e estrelas de comparación a partir das súas coordenadas celestes.

Empregando unha fotometría de apertura adaptativa, que permite configurala de acordo ás condicións de seeing, obteranse as magnitudes instrumentais dos sistemas binarios e as súas estrelas de comparación, que permitirán levar a cabo a fotometría diferencial. Tras isto, diferentes técnicas de computación posibilitarán a obtención dos instantes das eclipses primarias durante as noites de observación; desta maneira, lograranse calcular os períodos dos diferentes sistemas binarios a través da ecuación de efemérides. Finalmente, empregando os resultados de instante de inicio das efemérides e o período, obteranse as curvas de luz dos sistemas binarios eclipsantes.

Contents

1 Introduction **3**

1.1 Counts number and signal-to-noise ratio . . . 3

1.2 Image formation: PSF and seeing . . . 4

1.3 Aperture photometry. . . . 5

1.3.1 Differential photometry . . . 6

1.4 Eclipsing binary star systems . . . 6

1.4.1 Heliocentric Julian date . . . 7

1.4.2 Ephemeris equation . . . 7

2 Design and preparation of eclipsing binary star observations **7**

2.1 Object selection and time allocation . . . 7

2.2 Observation preparations . . . 8

2.3 Observation with the IAC80. CAMELOT2 . . . 9

3 Observation process **12**

3.1 The bias . . . 12

3.2 The flat-fields . . . 12

3.3 Observation details . . . 13

3.3.1 Auto-guiding process . . . 13

3.3.2 Binary star systems observation . . . 13

4 Photometric data reduction and astrometry process **14**

4.1 Data reduction . . . 14

4.2 Reduced images astrometry . . . 15

5 Adaptive aperture photometry in `Pyraf` **16**

5.1 Differential photometry with `Phot` . . . 17

6 Period calculation and light curves obtainment **17**

6.1 Monte Carlo simulation . . . 18

6.2 Light curves analysis 19

7 Conclusions **20**

8 Appendix **22**

8.1 Observation nights description 22

8.2 Images reduction results and time instants of the eclipses 23

1 Introduction

One of the basic astronomical objectives throughout history has been to determine the amount of flux emitted by a celestial object in a certain wavelength interval. This process, called photometry, constitutes one of the main branches of astronomy [1]. As early as the 2nd century BC, Hipparchus of Nicaea divided the visible stars into six classes according to their apparent brightness; if the flux densities of three stars are in the ratio 1:10:100, the brightness difference of the first and the second star appears to be the same as the last two. This logarithmic human perception of brightness inspired the definition of apparent magnitude, which is that brightness that shows the celestial object as it is seen in the sky, regardless of its temperature, its size or distance from the object

$$m = -2.5 \log_{10} \left(\frac{F}{F_0} \right) \tag{1}$$

For this definition, we have taken as reference the spectrum of a known star and defined it with magnitude $m_0 = 0$ for its flux density F_0.

One of the most important elements to be taken into account when correcting the astronomical objects magnitudes is the atmosphere, since it performs selective light absorption and scattering. This atmospheric extinction, due to steam and aerosols in its different air layers (among other things), mathematically translates as

$$m_1 - m_0 = -2.5 \log_{10} \left(\frac{F_1}{F_0} \right) - k \cdot z \tag{2}$$

where F_1 and F_0 are the celestial objects fluxes measured in the presence of Earth's atmosphere, k is the atmospheric extinction coefficient in [mag/air mass] and $z = z_1 - z_0$ is the air mass difference of the atmosphere at which the observations of the two objects are made.

1.1 Counts number and signal-to-noise ratio

The CCD (Charge Coupled Deviced) sensor is the telescope element that allows to detect the number of photons per unit of time that enters in optical system and, therefore, records the sky image observed by the telescope; thus, we must find a relationship between magnitudes and counts. Considering that the energy of a photon of wavelenght λ is determined by

$$E = h\nu = h\frac{c}{\lambda} \tag{3}$$

where h is the Planck's constant and c is the light speed in vacuum, the number of photons per second N regarding to the flux can be defined as

$$N(\lambda) = F(\lambda) \frac{\lambda}{hc} \tag{4}$$

Taking into account the above relationship, Equation 2 is rewritten as

$$m_1 - m_0 = -2.5 \log_{10} \left(\frac{N_1}{N_0} \right) - k \cdot z \tag{5}$$

with N_1 and N_0 the number of counts, in a given filter, for the celestial object and for the calibration star respectively.

An extremely important figure of merit that evaluates the quality of the photometric measurement provided by the CCD is the signal-to-noise ratio (S/N) [2]. This figure of merit is given by the so-called "CCD Equation", mathematically described as

$$S/N = \frac{N_*}{\sqrt{N_* + n_{pix} \left(N_S + N_D + N_R^2 \right)}} \tag{6}$$

where N_* is the number of photons captured by the CCD for a given object, n_{pix} the number of pixels which capture the N_* photons, N_S the number of sky background photons, N_D the total number of dark current electrons per pixel and N_R the total number of electrons per pixel resulting from readout noise.

If the total uncertainty for a given measurement $\sqrt{N_* + n_{pix}\left(N_S + N_D + N_R^2\right)}$ is dominated by the source noise, the CCD equation simplifies to

$$S/N = \frac{N_*}{\sqrt{N_*}} = \sqrt{N_*} \tag{7}$$

expression that concurs with the error σ associated to a variable that follows the Poisson distribution ($1\sigma = \sqrt{N}$). Therefore, we can consider that Equation 6 is given by the signal N_* divided by the sum of a number of Poisson noise terms.

1.2 Image formation: PSF and seeing

According to Fraunhofer's diffraction theory for a point object [3], optical systems provide the Fourier transformation of the intensity distribution at the exit pupil (pupil function). Since telescopes, in general, have a circular pupil, its intensity image will be the PSF (Point Spread Function). That is, when imaging with a telescope, the result is the PSF, which provides the intensity profile of the point source.

In this case, the FWHM (Full Width at Half Maximun) will be determined by the telescope diffraction limit of diameter D

$$\theta_{FWHM} = 1.22\frac{\lambda}{D} \tag{8}$$

For long exposure times and in the presence of atmospheric turbulence, the intensity disk to be obtained for a point object image is the seeing disk, which will be a Moffat distribution[1]. Therefore, seeing (S) is defined as the parameter that indicates the quality of a celestial object image and provides information about the distorting effect of the atmosphere.

$$S = \theta'_{FWHM} = 0.98\frac{\lambda}{r_o} \tag{9}$$

being $r_0 \propto \lambda^{\frac{6}{5}}$ the Fried's parameter. It is important to emphasize that observations with telescopes of diameter $D > r_0$ will always be limited by seeing (approximately in telescopes of diameter greater than 20-30 cm).

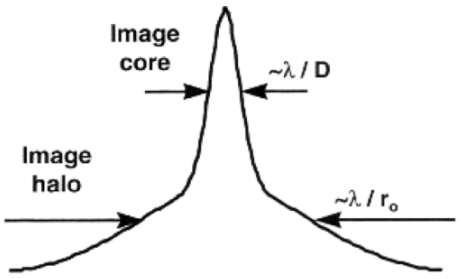

Figure 1: Point Spread Function (PSF) of a point object at infinity in a telescope of diameter D and in presence of the atmosphere. The atmosphere effect is reflected in the image halo, proportional to the Fried's parameter r_0.

[1] Moffat distribution: continuous probability distribution based on the Lorentzian distribution incorporating seeing-dependent parameters.

According to Figure 1, as the seeing increases so will the FWHM. This translates in the image as a reduction of the number of counts in the center of the PSF, meaning, photons coming from the celestial object are scattered along the seeing disk.

1.3 Aperture photometry.

Aperture photometry is a technique that takes into account only the number of counts within a specific aperture centered on the source, without considering the actual PSF shape of the object.

First, to perform this type of photometry, the celestial object PSF center must be estimated and then, a circular aperture[2] of radius r around that center must be inscribe [2]. According to Equation 6, to obtain a higher S/N ratio it is necessary to collect more signal from the source N_*; in this case increasing the aperture radius up to a maximum of 3·FWHM (Figure 2), with which practically 100% of that signal is contained.

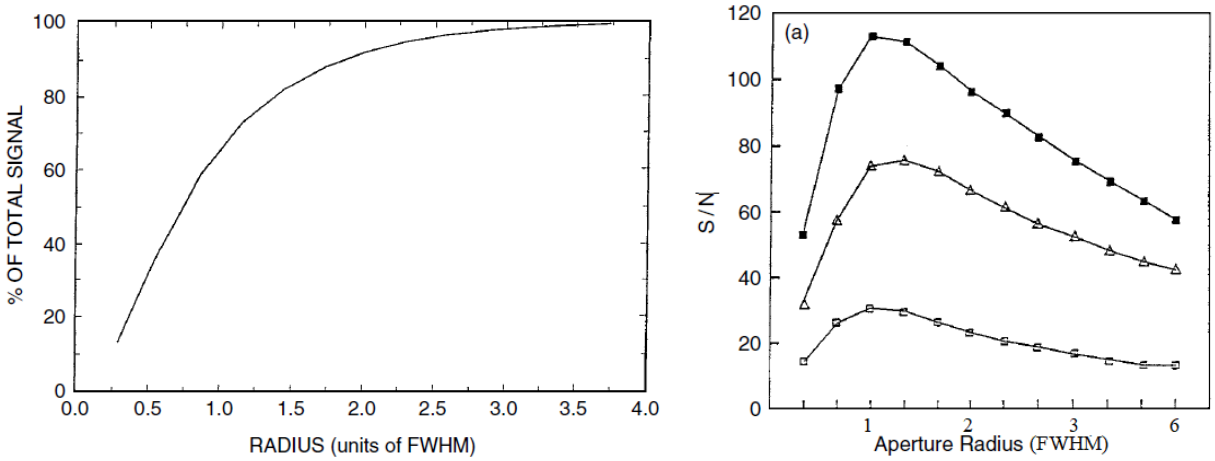

Figure 2: Left: Relationship between the contained source signal and the aperture radius. Right: Relationship between the signal-to-noise ratio and the aperture radius; this last plot represents the idea of optimal radius for three point sources that differ in brightness by magnitudes of 0.3 (middle curve) and 2.0 (bottom curve) compared to the top curve [2].

However, the larger r is, the more n_{pix} are included within the aperture. Thus, as this value increases, the greater the contribution of noise sources to the signal error. Therefore, an optimal aperture radius that maximizes the signal-to-noise ratio must be sought , that is to say, a radius that balances the signal that is incorporated into the photometry and the noise that is associated with the pixels that set up the aperture. An optimum aperture radius can be determined for any PSF and, in general, has a value close to 1·FWHM (Figure 2).

Moreover, it must be taken into account that the signal collected by the aperture does not correspond exclusively to photons from the analyzed celestial source, but also to photons from the sky background; this is why this additional signal must be estimated and eliminated before performing the photometry. To determine this background level, a ring is placed around the aperture, characterized by two variables: the annulus, which corresponds to the inner radius of the ring, and the dannulus, which defines its width. To correctly determine the local background variations, the sky ring must be close to the source without containing any signal from it, that is why the annulus must have a value of about 4· FWHM (Figure 2).

[2]The circular aperture is the usual geometric shape, as it is used for point source photometry.

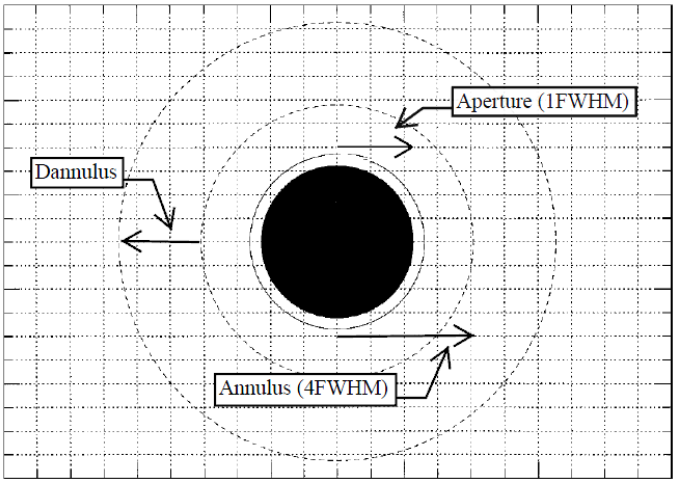

Figure 3: Schematic drawing of a stellar image on a CCD pixel grid [2].

1.3.1 Differential photometry

Differential photometry deals with the measurement of the difference in brightness between one or more astronomical sources compared to one or more comparison celestial objects that are in the same telescope's FOV (Field of View). That is, the final result of this type of photometry is a relative measurement, since it is only known with respect to other sources.

Differential photometry allows that the relationship between the studied objects fluxes to be unaffected by seeing, the atmosphere air mass or the clouds passage, for example; if these elements affect part of the light during an exposure, they will influence in the light of the comparison stars and the object under study by the same fraction, since they are close together in the sky.

1.4 Eclipsing binary star systems

Many of the stars we observe in the firmament form a physical system, in which two or more stars orbit around a common center of gravity; in fact, it is estimated that less than 50% of the stars are single elements such as the Sun [4].

Among the different types of binary stars that exist, eclipsing binary star systems are particularly interesting. This type of binary is a system formed by two stars whose orbital plane is oriented towards the Earth, so that, from our perspective, they undergo eclipses and mutual transits.

The study of these binary systems by analyzing their light curves (periodic variation of their magnitude due to its components passing one in front of the other in our line of sight) is very important because it allows to determine, with great precision, the values of their physical parameters. The analysis of these light curves at different wavelengths, combined with radial velocity measurements (determined with spectroscopic techniques), allows to define parameters such as radii, masses and temperatures of the binary components (among others), that would otherwise be much more complex to determine. In addition, the stellar parameters obtained enable to know the evolution state of the stars in the system.

1.4.1 Heliocentric Julian date

Since the commonly used date format is not useful for timing astronomical events, it is usual to use the Julian date, which gives the number of solar days that have elapsed since 12 UT on January 1, 4713 BC from Greenwich.

In addition, a correction is necessary to offset the movement of the Earth around the Sun: a star on the far side of the Sun requires nearly 16 more minutes for its light to reach the Earth than when the Earth is on the same side of the Sun as that star, approximately six months later. This correction, together with the Julian date, defines the heliocentric Julian date (HJD).

1.4.2 Ephemeris equation

Since the light curve of an eclipsing binary star system is usually periodic, the eclipse moments can be calculated by using a linear ephemeris equation

$$HJD_{min} = HJD_0 + P_0 \cdot E \tag{10}$$

in which:

- HJD_{min} is the primary eclipse time.
- HJD_0 is a time instant that establishes the origin of the ephemeris.
- The orbital period P_0 is the revolution time of the binary stars around the center of mass.
- E is an integer.

2 Design and preparation of eclipsing binary star observations

2.1 Object selection and time allocation

In 2002, it was published "*The All Sky Automated Survey. Variable Stars in the* 0^h - 6^h *Quarter of the Southern Hemisphere*", which collects the binary systems identified from the photometric data of the ASAS cameras monitoring the entire V-band sky [5]. Also, in 2007, it was published "*Identification, classification and absolute properties of 773 eclipsing binaries found in the trans-atlantic exoplanet survery*" in which a method for the systematic analysis of photometric data (obtained during the search for exoplanets) is presented [6]. From this two papers, the eclipsing binary star systems detailed in the following table were selected.

Table 1:
Observational parameters of the binary star systems studied in this work [7].

Binary star system	α (J2000[3])	δ (J2000)	**Period** [d]	**Magnitude range** (V filter)
2MASS J01074282+4845188 [4]	01 07 42.83	+48 45 18.8	0.1935980	15.0 - 17.2
ASAS J052919-1617.3	05 29 19.32	-16 17 18.7	0.660855	11.252 (0.191)

[3] J2000 refers to the Julian equinox, which is used as a reference for calculating the coordinates of celestial bodies.
[4] Also known as T-And0-10518 and thus referenced in [6].

The selection criteria of the binary systems has been based on the visibility of the objects during the available observation months, their short orbital period (which will allow us to observe the complete light curves) and their magnitudes, which must be suitable for the instrumentation of the telescope.

To perform differential photometry, comparison stars, which are in the telescope's FOV close to the binary systems, must be selected. These comparison stars must have a binary-like brightness to avoid saturation of any of the selected celestial objects. That is, if any of our objects is not very bright, we would need a long exposure time to reach a suitable number of counts; however, the brighter object would eventually saturate (see Section 2.3).

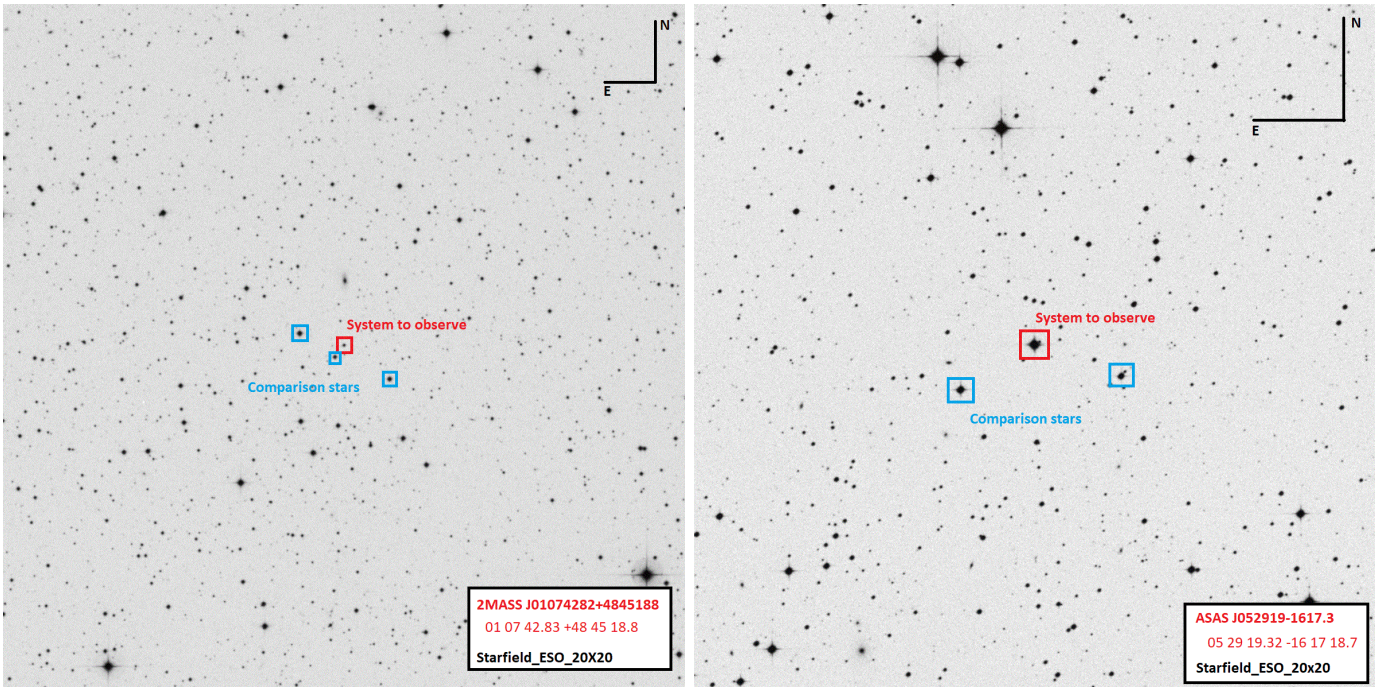

Figure 4: Binary star system starfield of 2MASS J01074282+4845188 (left) and ASAS J052919-1617.3 (right) [8].

Once the binary systems and their comparison stars have been chosen, the instants of the binary stars eclipses are calculated through the ephemeris equation [7], determining when the primary eclipses take place and which phases of the light curve are observed each night. Once this is done, the study proposal of the two binary systems is elaborated with the chosen observation nights to complete their light curves.

The observation times allocation in the IAC80 telescope was made through the IAC (Instituto de Astrofísica de Canarias) once the study proposal was validated. The nights granted were a total of 12, distributed between the months of November 2020 and January 2021, as detailed in Table 7 (Section 8.1).

2.2 Observation preparations

Due to celestial dynamics, it is not possible to study any object at any time. The observation interval of a given celestial body is limited, first, by the date and location of the telescope and, second, by the limitations of the telescope itself.

The IAC80 imposes a minimum object altitude of 30° over the horizon for pointing and later observation. This restriction is due to, on the one hand, a structural reason: below this limit, certain mechanical stresses are produced on the telescope mirrors and it would be necessary to carry out recalibrations on the telescope

systems. On the other hand, below that height, the air mass begins to increase significantly, greatly affecting the quality of the images.

Taking into account these limitations, and once the objects elevations above the horizon throughout the night are known (Figure 5), the assigned nights were divided into three parts:

- Previously and during evening twilight, two types of calibration images were taken: bias and flat-fields.
- During the first part of the night the 2MASS J01074282+4845188 system is observed.
- ASAS J052919-1617.3 binary begins to be observed in the second part of the night, when it is 30° over the horizon.

Due to its period (15.86 h), ASAS J052919-1617.3 should be observed as long as possible to obtain the most data from its light curve each night. From 2MASS J01074282+4845188 system, with a period $P_0 = 4.65$ h, almost all of its phases are observed in a single night.

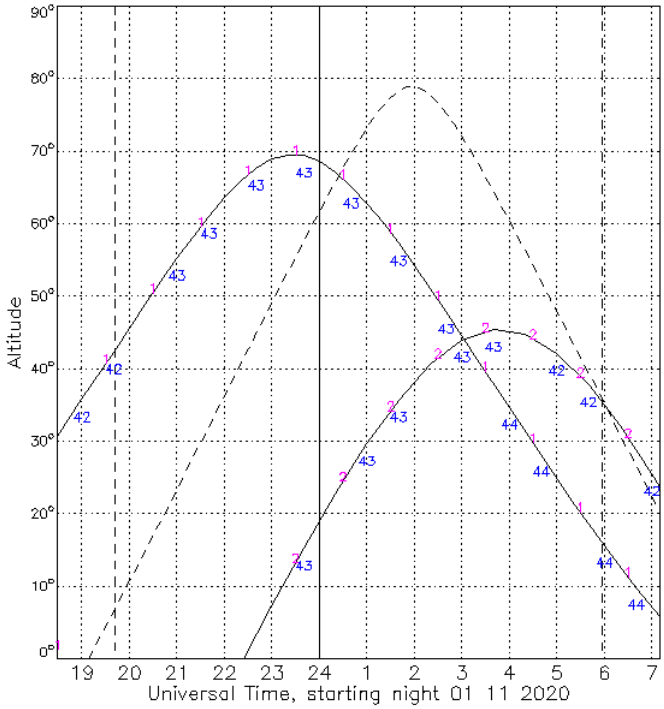

Figure 5: Binary systems altitude over the horizon against time plot for November 1, 2020. Line 1 corresponds to the 2MASS J01074282+4845188 binary system, while line 2 corresponds to the ASAS J052919-1617.3 binary system. The dashed line indicates the sky position of the Moon throughout the night; on the other hand, the vertical dashed lines indicate the evening and morning twilight [9].

2.3 Observation with the IAC80. CAMELOT2

Observations were made using the CAMELOT2 camera (CAmara MEjorada Ligera del Observatorio del Teide) placed in the Cassegrain focus of the IAC80 telescope at the Observatorio del Teide [10]. This CCD, sensitive to the visible range, has a matrix of 4096x4096 pixels of 15 μm each, providing a pixel scale in the sky of 0.336 arcsec/pixel and a FOV of 23x23 arcmin.

CAMELOT2 has 5 readout modes, each one associated with 4 different readout speeds and observing characteristics. The chosen mode was 0 because, taking into account the magnitudes of the two binary systems and their comparison stars, it allows to obtain an optimal signal-to-noise ratio and deviation from linearity to perform differential photometry [11].

The exposure time is very relevant to avoid saturation of the CCD. This is because each pixel in the camera has a maximum capacity to store electrons, and the longer the exposure time, the more photons are accumulated. Beyond this limit, the capture of more photons creates more electrons that are placed along a pixels column of the CCD; thus, vertical streaks, that spoil the information stored in adjacent pixels and cause loss of information from the saturated pixels, are created.

Table 2:
CAMELOT2 readout modes at its operating temperature T = -105°C [10].

Mode	**Readout speed** [kHz]	**Readout time** [s]	**DR** [ADU]	**Gain** [5] [e^-/ADU]	**Readout noise** [ADU]
0	344 (Attn 0)	13.5	56000	4.11	6.76
1	344 (Attn 1)	13.5	40000	7.76	10.99
2	709	7.2	22000	9.78	13.99
3	100	43.6	60000	0.78	6.27
4	855	6.6	12000	19.94	25.27

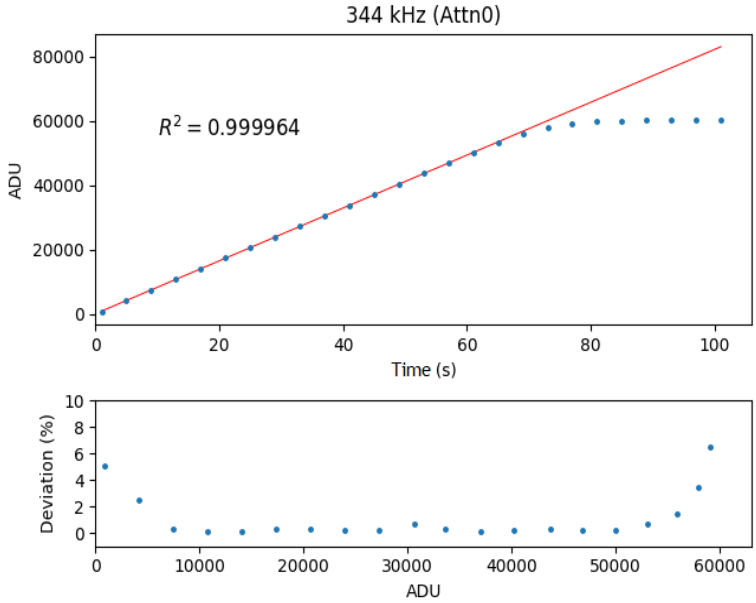

Figure 6: CAMELOT2 linearity for mode 0. Its dynamic range is 56000 ADU (counts) [10].

The CCD must operate in an interval where the detector's output signal is linear compared to the intensity generated in the reading process: this interval is called the Dynamic Range (DR) (Figure 6). In consequence, during the measurement process it is crucial that both, the binary system and the comparison stars, are kept below 56,000 counts, that is, within the CAMELOT2 DR.

To limit the set of wavelengths entering the detector, the IAC80 has a 12-position filter wheel, each one with different associated wavelengths and band-passes. In our study, we will use the V, R and I filters of the Johnson-Bessell system, located on said wheel in positions 3, 4 and 5 respectively (Table 3). These filters

[5] Gain = $\frac{e^- \ per \ pixel}{counts \ per \ pixel}$

were chosen because the Johnson system was designed to measure certain fundamental stellar parameters, such as effective temperatures [6] and the surface gravity of stars.

It is important to mention that, as a result of having recycled the filter wheel of the old IAC80 CCD camera, CAMELOT2 images show significant vignetting. This means that there is a decrease in the luminous flux distribution that reaches the focal plane as we move away of the optical axis, caused by the finite size of the system aperture. As a result of this vignetting, there is a reduction in the telecope field of view (Figure 7).

Table 3:
Filters used during observations [10].

Filter	**Effective central wavelength** [nm]	**Width** $\Delta\lambda$ [nm]	**Maximun transmission** (%)
V	537.40	84.60	86.75
R	627.25	127.30	82.04
I	872.20	298.00	93.70

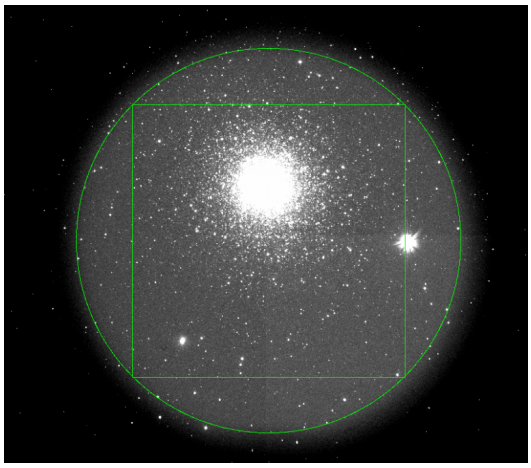

Figure 7: Vignetting of the images taken with CAMELOT2 in the IAC80. The green circle has a diameter field of 17.3 arcmin and the square has a field of 12.3×12.3 arcmin^2. [10].

Imaging using a CCD camera, such as CAMELOT2, involves readout noise (RON), which introduces an additional number of electrons into the CCD electron count. This is due to the fact that, after an exposure, amplifiers are involved in the CCD readout process, which generate electrons randomly.

Furthermore, if we allow the CCD to run for a certain exposure time without radiation hitting upon it, there will be a signal as a result of its operating temperature; this is known as the dark current. This current is also very sensitive to temperature and, due to CAMELOT2 cooling, we will consider it negligible in our measurements.

There is also another inaccuracy source in CCD measurements because of the different Quantum Efficiency (QE) in the pixels: uniform illumination will not generate an equal signal in each camera pixel (even ignoring readout noise and dark current). As the quantum efficiency of each pixel depends on the wavelength, it will vary according to the type of incident electromagnetic radiation.

Finally, the celestial objects PSF shape in CAMELOT2 elongates as they approach the lower left corner of the detector. This will not be a problem in our observations since the binary star systems will be located around the detector's center and their comparison stars are close to them in the image.

[6] Effective temperature: Black-body temperature that radiates the same total flux density as the star.

3 Observation process

3.1 The bias

To ensure that a negative number of counts will never appear in images taken with a CCD (due to readout noise), an artificially roughly constant level of counts is introduced with the bias, for all pixels and regardless of the exposure time. Besides, since the bias signal is generated on the CCD at zero exposure time, it will be independent of the filter used.

In addition, there is a part of the CCD that is not exposed, known as overscan, which allows a bias value to be obtained at the same time as the data is acquired. It should be noted that the bias images provide the spatial distribution of the level of counts introduced, while the overscan provides the temporal variation of these counts in certain columns.

The bias measurement with the IAC80 is performed by closing the telescope petals, shutting the camera and at zero exposure time. Also, per IAC80 protocol, the telescope must be pointed at the zenith and with the dome lights off. Then, a set of bias images are obtained.

3.2 The flat-fields

Flat-fields are images of a uniformly illuminated field that are used to correct pixel-by-pixel variations in quantum efficiency and non-uniform illumination in the focal plane, caused by the optical system itself and by dust spots and specks. Since the quantum efficiency of each pixel is a function of the wavelength and each filter has its dust pattern, each of them will have its corresponding flat-field.

Flat-fields are measured at twilight for a sufficient exposure time to achieve the appropriate number of counts, which depends on the readout mode used. Using the 50% dynamic range criterion, for readout mode 0, flat-fields should have approximately 28000 counts.

This criterion was chosen over others because the most linear part of the camera is located in the middle of the dynamic range (Figure 6) and it will be here where deviations from the linear regression are best detected. Besides, this guideline allows making room for hot pixels (pixels with a high number of counts compared to the rest) and for the variation in brightness in the dome flats (due to lights heating and spotlights).

Two types of flat-fields were taken during the observations: dome flats and sky flats. Dome flats are exposures of an artificially lit screen inside the dome of the telescope. To take this type of flat-fields, first, the telescope must be pointed to the south, and then, the dome must be moved so that the white screen occupies the entire FOV of the camera. The screen illumination is done using two lights (red and white) and two spotlights (spotlight 1 and spotlight 2), whose settings, provided by the IAC, depend on the filter and the readout mode of CAMELOT2.

Sky flats are taken by observing a uniform light portion of the sky at twilight. To do this, the telescope is pointed at 45° above the horizon to the opposite zone to sunset, that is, to the east during evening twilight. Since the path that light follows when making dome flats differs from that of observing the sky and, since the screen illumination may show brightness gradients, it is preferable to take sky flats rather than dome flats. However, sky flats have been found to have a number of drawbacks:

1. A completely clear sky is required. The presence of cirrus clouds or haze (if it is not uniform) over the observatory prevents a uniform light distribution.

2. Since twilight at the Observatorio del Teide lasts approximately 30 minutes in the observation months [13], it is difficult to get enough sky flats in all filters.

3. Since exposure times have to be continuously adjusted to the change in sky brightness, the variations in count levels between flat-fields of the same filter are larger than those appearing in the dome flats. This means that the rejection algorithms are less efficient and the signal-to-noise ratio in the combination of sky flats cannot be scaled as $\sqrt{n \cdot ADU}$, where n is the number of taken flat-fields.

Given the drawbacks imposed by the short duration of twilight, why have not flat-fields been taken with a shorter exposure time and higher illumination? This is due to shutter effects on images: the finite opening and closing time of this element changes the illumination throughout CAMELOT2. There is a non-linear behavior of the number of counts up to, approximately, 70 ms, where the shutter aperture effects end.

3.3 Observation details

3.3.1 Auto-guiding process

After taking the bias and flat-field images, the coordinates of the binary system are entered into the telescope system and its tracking is programmed, thus the rotational movement of the Earth is compensated. In addition, the FOVIA auto-guiding tool must be configured, which detects small tracking drifts for later corrections using an auxiliary camera and a guide star (easily distinguishable star).

3.3.2 Binary star systems observation

After having pointed to the corresponding binary star system and configured the auto-guiding, a series of "test" images are taken in order to determine the exposure time to be used in each filter. The number of counts indicated in Table 4 corresponds to the PSF center of the binary star system, where we will have a greater number of them.

2MASS J01074282+4845188: For an exposure time of 60s, a reduced number of counts was obtained. If the seeing gets worse, the counts will be reduced and could be camouflaged by the sky background noise: for this reason the exposure time should be increased to 180s. However, it should be noted that the number of counts in V filter is about half compared to the R and I filters; this means that to obtain the same number of counts, the exposure time in V filter should be twice the other two exposure times, causing a significant loss of temporal resolution in the light curves. Therefore, the 2MASS J01074282+4845188 system will only be studied in filters R and I.

ASAS J052919-1617.3: For this system, the exposure time in the test was reduced with respect to the other because it has a smaller magnitude. Since these exposures were made when the object is at 30° over the horizon (in presence of a greater air mass and, consequently, worse seeing), the increase in the number of counts as the nights go on must be taken into account. Therefore, looking at that night moment for 30,000 counts in each filter (to avoid saturation on the binary star and its comparison stars as they ascend in the sky), the exposure times indicated in the last column of Table 4 were used.

Relevant comments about different observation days are detailed in Section 8.1.

Table 4:
Exposure times used in the observations.

Binary star system	**Filter**	**Exposure time TEST** [s]	**ADU**	**Exposure time** [s]
2MASS J01074282+4845188	V	60	1624	-
	R	60	2556	180
	I	60	2743	180
ASAS J052919-1617.3	V	10	3067	100
	R	10	6529	45
	I	10	12077	25

4 Photometric data reduction and astrometry process

4.1 Data reduction

The CCD data reduction process consists in the elimination, by means of computational techniques, of the effects caused by the instrumentation that change the information obtained during the observation. This process consists in correcting the astronomical images of type "object" from the bias and flat-field images taken.

CCD detectors provide an output signal S, which depends on the exposure time t_{exp} and the energy and orientation of the photons received at the CCD. Mathematically, the S expression for each pixel, located at position (x,y) in the image, is given by:

$$S(x,y) = B(x,y) + [O(x,y) + F(x,y)I(x,y)]\, t_{exp} \tag{11}$$

in which $B(x,y)$ is the bias term, $O(x,y)$ the dark current, $F(x,y)$ the mean normalized flat-field term and $I(x,y)$ the final corrected pixels, given in number of photons per unit of time. Solving for the $I(x,y)$ term from Equation 11 and ignoring the $O(x,y)$ term (negligible for CAMELOT2), the value of the corrected pixel is:

$$I(x,y) = \frac{S(x,y) - B(x,y)}{F(x,y)} \cdot \frac{1}{t_{exp}} \tag{12}$$

As already indicated, at the beginning of the observation a set of bias and flat-field images are obtained. Thus, to apply Equation 12, it must be taken into account that $B(x,y)$ and $F(x,y)$ terms will be a combination of all bias and flat-fields, called masterbias and masterflat respectively.

The reduction process has been performed with `IRAF` (Image Reduction and Analysis Facility), a collection of software developed by the NOAO (National Optical Astronomy Observatory) and dedicated to the processing and analysis of data provided by CCDs. The reduction tasks have been accessed through the `PyRAF` environment, which allows calling the `IRAF` software from `Python` [14].

Schematically, the programming process has been designed as shown in Figure 8. The masterbias has been obtained using the software `imcombine`, with a pixels rejection method based on the "minmax" algorithm using the mean as a combination mode. The masterbias subtraction from the flat-fields and the "object" images and its trim is done with `ccdproc`, without taking into account neither the dark current nor the overscan zone (since this zone is not implemented in CAMELOT2). On the other hand, the obtaining process of the different masterflats (one per filter) is carried out with the `flatcombine` package: in this case, no rejection method has been applied, since the median is used as the flat-fields combination variable. The

median is a very illustrative statistic of the pixel counts distribution that allows to reject cosmic rays, hot pixels, and stars that may appear in each flat-field. The result of this combination is then normalized using the mean, obtaining the masterflats. Finally, the "object" images with the subtracted masterbias are divided by its corresponding masterflat, taking into account with which filter they were taken.

The data reduction results are detailed in Section 8.2 (Table 8).

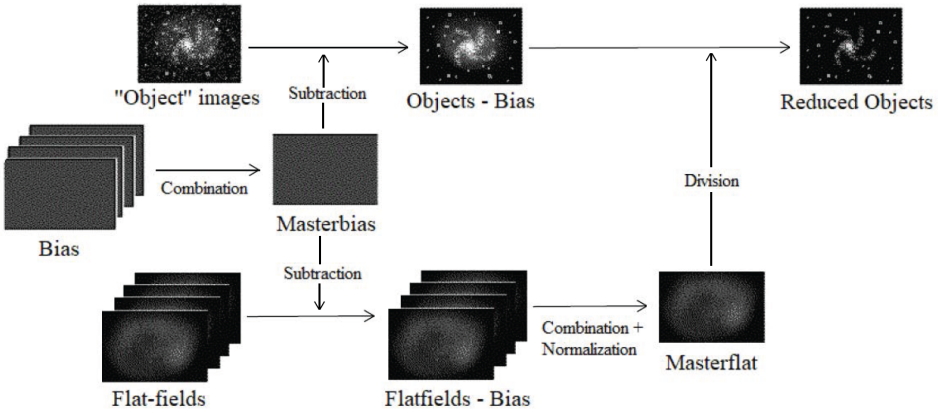

Figure 8: Photometric data reduction process.

4.2 Reduced images astrometry

Despite having configured the telescope to compensate Earth's rotation and system drifts in pointing, it is necessary to map the images to obtain a relationship between the celestial coordinates and the position (x,y) of each pixel.

To do this, using `PyRAF`, a computer program is made using four software packages: `starfind`, `fitpsf`, `ccxymatch` and `ccmap`. The first one automatically locates the stars present in the images as well as their position (x,y). Two critical parameters in this software must be taken into account:

- To determine the detection threshold, 3 times the standard deviation of the sky has been taken. This ensures that we will be able to discard most of the hot pixels that may interfere with the detection within a 99% confidence interval.
- `Starfind` requires a FWHM value used to analyze the celestial objects of the image. To determine it, the first image taken for each filter and object has been analyzed using the `imexam` tool: in an arbitrary way, fast radial profile adjustments of unsaturated stars have been performed and an average has been made with the FWHM values obtained. The choice of these "object" images is due to the fact that, at the beginning of the night, the FWHM is, in general, worse than during the rest of the night because hot air is still present in the observatory and within the dome itself.

Once the stars of the "object" image have been located, using the `fitpsf` package we obtain the FWHM of each of them and its value is compared with the star instrumental magnitude given by `starfind`. In Figure 9 it can be seen that there is a detection limit for objects with magnitude greater than about -8.5. Once the radial profile of these objects has been analyzed, we can conclude that they are not stars, but hot pixels or cosmic rays. In addition, close to this detection limit, it can be seen that the FWHM increases, which may be due to two circumstances: because they are higher magnitudes, the software confuses between stars and large objects (e.g. galaxies) or because objects with lower brightness have a lower signal-to-noise ratio, increasing the uncertainty.

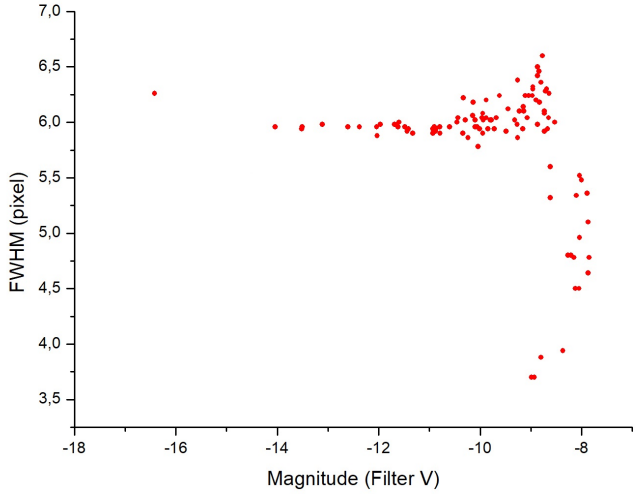

Figure 9: FWHM vs. magnitude of the celestial objects detected by `Starfind` on January 30 in the V filter for an ASAS J052919-1617.3 image.

Using the found stars with a magnitude value less than the limit mentioned above, the `ccxymatch` software generates all the possible triangles that can be formed from them. Then, it compares these triangles with those generated from a list of star coordinates obtained from the UCAC4 catalog [15], accessible through the VizieR database [16]. The matching triangles allow to generate a transformation function between pixel position (x,y) and equatorial coordinates, which is stored in the "objects" images header through `ccmap`.

5 Adaptive aperture photometry in `Pyraf`

After performing image reduction and astrometry, the next step is to perform the photometry of the two binary star systems and their comparison stars. For this, the `phot` package, included in `IRAF`, will be used.

Determining the FWHM of each image using the mode of the `fitpsf` data, we define in `phot` the fundamental parameters of the aperture photometry:

- As indicated in Section 1.3, aperture and annulus values are one time and four times the FWHM respectively.
- The dannulus value has been determined taking into account the signal-to-noise equation: by increasing the ring's width, we would be reducing the error made when estimating the sky background, but not evaluating the local sky of the celestial object. Finally, after different simulations, the dannulus value has been set in such a way that the sky ring has an area two hundred times the aperture area.

It is necessary to indicate to `phot` where the binary star system and the comparison stars are located to do the photometry on them. Introducing the equatorial coordinates of the celestial objects in the `cctran` package, these will be transformed into (x,y) image coordinates using the transformation function generated by `ccxymatch`.

Once the above values are set, the sky background is calculated using the "centroid" algorithm, which uses the histogram of the object's sky pixels whose mode is obtained by calculating its centroid. This algorithm has been chosen over others because it is reasonably robust in regions with rapidly varying sky backgrounds or populated zones with a high number of stars.

Finally, the HJD of each image is calculated using the `setjd` package. This software performs the calculation taking as time instant half of the exposure time of the "object" image and, as reference, the observatory where the observations were made.

5.1 Differential photometry with `Phot`

Once the photometry has been performed on all the "object" images of each observation night, we obtain for each of them different photometric data. For the study of our binary star systems, we will select the values of magnitude m and associated uncertainty m_{err} that the package `phot` calculates through the expressions

$$m = m_0 - 2.5 \cdot \log_{10}(F) + 2.5 * \log_{10}(t_{exp}) \quad ; \quad m_{err} = 1.0857 \cdot \frac{err}{F} \tag{13}$$

with

$$F = N - A \cdot m_{sky} \quad ; \quad err = \sqrt{\frac{F}{g} + A \cdot (std_{sky})^2 + \frac{A^2 \cdot (std_{sky})^2}{n_{sky}}}$$

In above equations m_0 is the magnitude scale origin, N the total number of counts in the aperture (including those from the sky background), A the aperture area in square pixels, m_{sky} and std_{sky} the sky background value per pixel and its standard deviation, t_{exp} the exposure time, g the gain in electrons per count and n_{sky} the number of pixels contained in the dannulus.

Using Equation 13, if m^c and m^b are the magnitudes of the celestial comparison object and the binary star system respectively, differential photometry gives us

$$\Delta m = m^c - m^b = -2.5 \cdot \log_{10}\left(\frac{F^b}{F^c}\right) \quad ; \quad \Delta m_{err} = \sqrt{(m^b_{err})^2 + (m^c_{err})^2} \tag{14}$$

6 Period calculation and light curves obtainment

Once the photometry has been performed, the differential data used will be those with a lower absolute value, in other words, we will take as the main comparison star the one whose magnitude is closer to the binary system magnitude.

The differential photometric data obtained in the different filters are plotting against time; from these plots, it is determined on which observation nights the primary eclipses took place and which data correspond to these instants of time.

The differential magnitude data of those eclipses are analyzed using the `scipy.optimize.curve.fit` software from `Python`, which performs a least-squares fit to polynomials of degree 3 to 7; the fit degree for each night and filter was chosen by taking into account the residuals distribution generated in each of them (Figure 10). Once the polynomial is selected, the minimum of the eclipse HJD_{min} is determined using `numpy.polynomial.polynomial.polyroots` and a robust uncertainty is generated through the Monte Carlo method [17]. Thus, the primary eclipses times of the binary systems in each filter have been calculated (Section 8.2, Table 9).

According to the linear ephemeris equation (Equation 10), for each binary star system a linear fit is conducted with their primary eclipse instants of all filters, obtaining their respective periods. Finally, the first observed primary eclipse has been chosen as the ephemeris origin HJD_0, taking the mean value of the filter data.

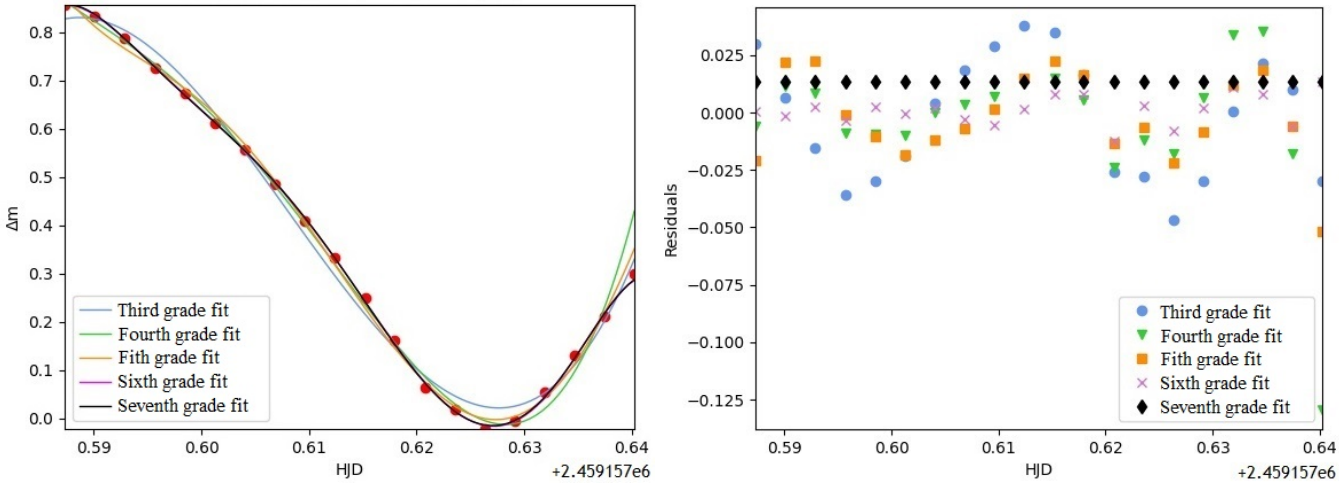

Figure 10: Adjustment of the filter R primary eclipse differential photometric data and generated residuals of November 4, 2020 (ASAS J052919-1617.3).

Table 5:
Ephemeris equation parameters of the observed binary star systems.

Binary star system	P_0	HJD_0
2MASS J01074282+4845188	0.193597038 ± 0.000000034	2459155.47614 ± 0.00012
ASAS J052919-1617.3	0.660825624 ± 0.000000020	2459155.643838 ± 0.000085

Once the parameters that characterize the ephemeris equation of each binary star system have been calculated, we can obtain their light curves directly from this equation, using that the phase, Ph, of each magnitude datum is given by the expression

$$Ph = x - [x] \qquad ; \qquad x = \frac{1}{P_0} \cdot (HJD - HJD_0) \tag{15}$$

where $[x]$ is the integer-part function of x.

6.1 Monte Carlo simulation

The Monte Carlo simulation for uncertainty propagation of the primary eclipses instants consists of taking as inputs the uncertainty distribution for each magnitude datum and the equation that allows to obtain the minima of the adjusted polynomial.

In each interaction, from each magnitude value a new one is generated randomly following the normal probability distribution, taking the original magnitude value as the distribution mean and its associated uncertainty as the standard deviation. Then, the new eclipse magnitude data is fitted to a polynomial of equal degree to the one chosen to fit the original data. Finally, the eclipse minimum is solved.

After 10,000 interactions, the uncertainty of the calculated primary eclipse instant is obtained by taking the width of the data distribution (got in said interactions) as its robust uncertainty.

6.2 Light curves analysis

At first, for the ASAS J052919-1617.3 system, the left light curve of Figure 11 was obtained; after the eclipses, this light curve shows data that clearly deviates from the trend of the rest. Adjusting the binary system to a Moffat function through the `imexam` package of `IRAF` in an "object" image, its radial profile shows that, from a radius of 5 pixels around its center, there are points/measurements that do not fit the adjustment and come from another object.

Since the aperture of the different "object" images is adapted to the seeing (its value is equal to the FWHM of the image), counts introduced by that contaminating object will not be a systematic error; this contamination changes with time and must be eliminated. To do this, the photometry process is performed again by setting the aperture to a maximum value of 5 pixels, regardless of the seeing conditions of the image.

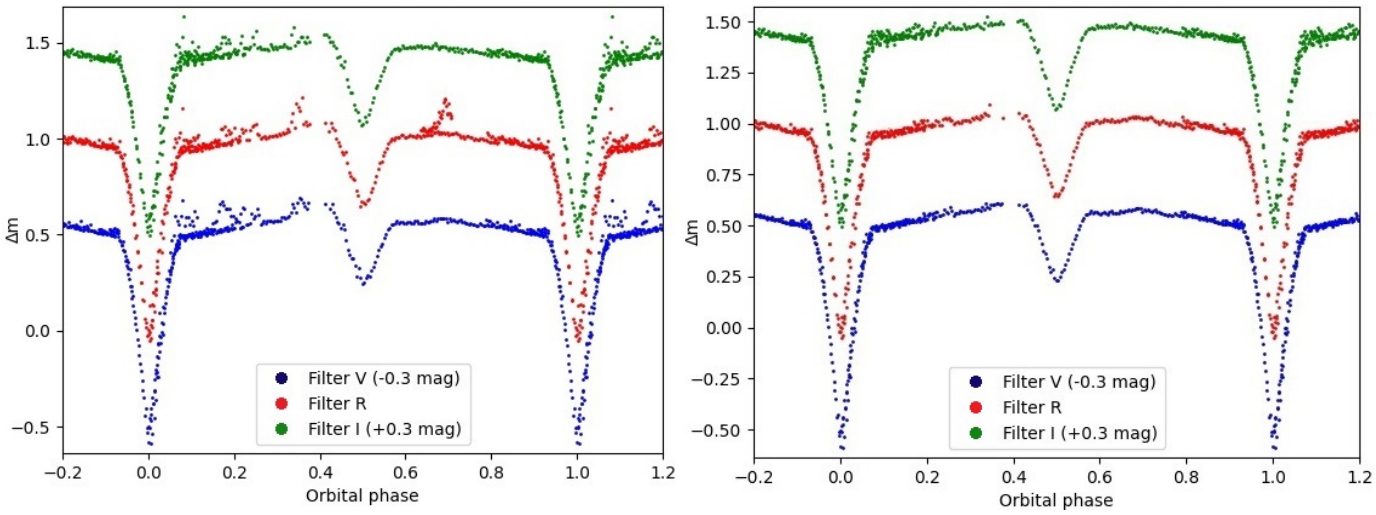

Figure 11: ASAS J052919-1617.3 binary system light curves. The figure on the left shows the result of the analysis without considering a contaminating object; the figure on the right represents the data obtained corrected from the presence of the contaminating object. Note that filters V and I light curves have been shifted to better viewing.

The light curve of the system 2MASS J01074282+4845188 presents, contrary to the previous one, two primary eclipses. Taking into account, in addition, the kind of splitting of the data outside the eclipses, we can corroborate that it is a cataclysmic eclipsing binary system [18]. These systems have their components in close proximity, with the secondary star (red dwarf) being distorted by the gravitational field of the primary (white dwarf); gas from the red dwarf forms the accretion disk, which surrounds the white dwarf until it falls into it.

The system's luminosity is dominated by the accretion disk luminosity, which depends on the mass that flows onto the outer parts of the accretion disk. Therefore, the light curve split data mentioned may be due to variations in the mass flux between the components of the 2MASS J01074282+4845188 system in the different observation nights.

In both binary star systems, V-shaped eclipses occur. For the ASAS J052919-1617.3 binary system, assuming that its elements are spherical, this means that they partially overlap.

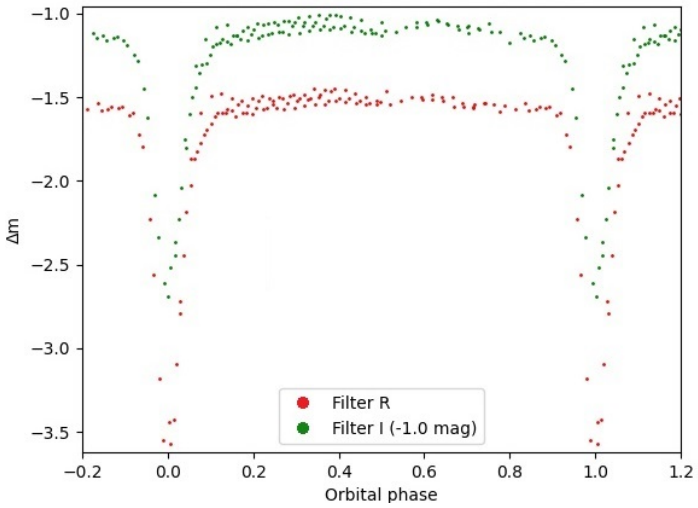

Figure 12: 2MASS J01074282+4845188 system light curve. Note that the light curve of filter I has been shifted to better viewing.

Finally, of particular note, in 2011 the paper *"2MASS J01074282+4845188: a new nova-like cataclysmic star with a deep eclipse"* [18] was published, in which a 2MASS J01074282+4845188 ephemeris equation is presented. As it can be seen in the Table 6, when obtaining the period of said system with the data of this work, it has been done with greater precision in terms of the number of decimal places. This is because, when making the linear adjustment, the primary eclipse HJD_0 that appears in the ephemeris equation of the mentioned paper has been included.

Table 6:
Comparison of the ephemeris equations obtained and those available in the literature.

2MASS J01074282+4845188	Paper [18]	2454417.382244 + 0.1935980 × E
	Own data	2459155.47614 + 0.193597038 × E
ASAS J052919-1617.3	AAVSO [7]	2451868.72 + 0.660855 × E
	Own data	2459155.643838 + 0.660825624 × E

7 Conclusions

Using the CAMELOT2 camera at the IAC80 in Observatorio del Teide, CCD images were obtained for two eclipsing binary star systems: 2MASS J01074282+4845188 and ASAS J052919-1617.3. After having reduced the images and accomplished their astrometry, it has been possible to perform the differential photometry of said binary systems. From the latter, their respective light curves have been obtained, as well as an update of their ephemeris equations.

It should be noted that, unlike with the 2MASS J01074282+4845188 system, for the ASAS J052919-1617.3 binary system its light curve has been obtained, for the first time, at different wavelengths, as well as an ephemeris equation acquired from a specific study of the object.

A more complete analysis of this last binary star system has been proposed as a Master's Thesis, in which near-infrared observations will be made to obtain its radial velocities using spectroscopic techniques. With the data presented in this paper and those obtained in these future observations, models of binary systems, such as the Wilson-Devinney model, will be applied to characterize the evolutionary state of the ASAS J052919-1617.3 binary system.

References

[1] Karttunen, H., Kröger, P., Oja, H. (2007). *Fundamental astronomy*, New York: Springer-Verlag Berlin Heidelberg.

[2] Howell, S.B. (2006). *Handbook of CCD Astronomy*, New York: Cambridge University Press.

[3] J. Scroeder, D. (2006). *Astronomical Optics*, California: Academic Press.

[4] Prsa, A. (2007). *PHOEBE Scientific Reference*, University of Ljubljana, Faculty of mathematics and physics.

[5] Pojmanski, G. (2002) The All Sky Automated Survey. Variable Stars in the 0^h-6^h Quarter of the Southern Hemisphere. *Acta Astron, 52,* pp.397-427.

[6] Devor, J., Charbonneau, D., T. Donovan, F., Mandushev, G., Torres, G. (2007) Identification, classifications and absolute properties of 773 eclipsing binaries found in the trans-atlantic exoplanet survey. *The Astronomical Journal, 135(3)*, pp.850-77.

[7] American Association of Variable Star Observers. *AAVSO: The International Variable Star Index.* https://www.aavso.org/vsx/

[8] ESO Online Digitized Sky Survey. *ESO Archive.* http://archive.eso.org/dss/dss

[9] Isaac Newton Group of Telescopes *Object Visibility - STARALT.* http://catserver.ing.iac.es/staralt/index.php

[10] Instituto de Astrofísica de Canarias: Observatorios de Canarias. *IAC80 Telescope.* http://research.iac.es/OOCC/iac-managed-telescopes/iac80/

[11] Instituto de Astrofísica de Canarias: Observatorios de Canarias. *CAMELOT2.* http://research.iac.es/OOCC/iac-managed-telescopes/iac80/camelot2-2/

[12] Romanishin, W. (2006). *An Introduction to Astronomical Photometry Using CCDs.* University of Oklahoma.

[13] Agencia Estatal de Metereología *Calendario Meteorológico 2020: Información meteorológica y climatológica de España.* http://www.aemet.es/documentos_d/conocermas/recursos_en_linea/calendarios/cm-2020.pdf

[14] National Optical Astronomy Observatory. *Software: IRAF* http://ast.noao.edu/data/software

[15] Zacharias, N., Finch, C.T., Girard, T.M., Henden, A., Bartlett, J.L., Monet, D.G., Zacharias, M.I. (2013) The Fourth US Naval Observatory CCD Astrograph Catalog (UCAC4) *The Astronomical Journal, 145(2)*, p.44.

[16] Centre de Données astronomiques de Strasbourg. *VizieR database* http://vizier.cfa.harvard.edu/viz-bin/VizieR

[17] Wall, J.V., Jenkis, C.R. (2003). *Practical Statistics for Astronomers*, New York: Cambridge University Press.

[18] Dimitrov, Dinko P., Kjurkchieva, Diana P. (2012) 2MASS J01074282+4845188: a new nova-like cataclysmic star with a deep eclipse. *New Astronomy, 1*, pp.34–37.

8 Appendix

8.1 Observation nights description

Table 7:
Relevant details of the observation nights of each binary star system.

Observation night	Binary star system	Observation [UT] Start	Observation [UT] End	Comments
01/11/2020	2MASS J01074282+4845188	20:00	01:05	- Refocus without stopping the observation to avoid the loss of the eclipse.
02/11/2020		19:55	01:30	- Delay in the beginning of the observation due to rain and presence of cirrus. - Bad seeing throughout the night.
03/11/2020		19:50	01:10	- Presence of streaks in the images due to the passage of satellites through the FOV.
01/11/2020	ASAS J052919-1617.3	01:15	06:20	- Seeing worsening around 01:30h. - Disconnection of FOVIA due to the passage of a cloud over its reference star
02/11/2020		01:45	06:10	- Bad seeing throughout the night. - Filter wheel error (05:45h): system reboot required.
03/11/2020		01:20	03:20	- Guiding problems detected in "test" images: FOVIA reconfiguration required - Observation interruption due to rainfall.
14/11/2020		-	-	- Yellow warning due to wind: cancellation of the observation.
15/11/2020		00:20	01:55	- Interruption of observation due to strong wind gusts.
19/11/2020		00:00	05:20	- Bad seeing throughout the night.
03/12/2020		-	-	- Rain, observation cancelled.
27/12/2020		21:20	02:50	- Ongoing filter wheel errors: Observation macro reconfigured
28/12/2020		21:30	02:50	- Ongoing filter wheel errors: Observation macro reconfigured
26/01/2021		20:10	00:50	- Bias and flat-fields measured at dawn.
30/01/2021		20:15	00:30	- Filter wheel error (22:05h): one hour of observation lost
31/01/2021		-	-	- IAC80 out of service.

8.2 Images reduction results and time instants of the eclipses

Table 8:
Results of the photometric data reduction.

Observation night	No. bias	Flat-fields				Masterbias		Masterflat (Stad. Dev.)		
		ADU (mean)	No. V	No. R	No. I	Mean	Stad. Dev.	V	R	I
01/11/2020	21	35000	21	21	21	498,40	0,84	0,018	0,014	0,017
02/11/2020	21	33500	21	21	21	498,40	0,90	0,019	0,014	0,017
03/11/2020	21	34000	21	21	21	503,30	1,35	0,017	0,014	0,015
15/11/2020	21	27500	11	11	11	498,10	0,88	0,019	0,015	0,018
19/11/2020	21	31500	11	11	12	498,30	0,82	0,017	0,012	0,015
27/12/2020	21	39000	-	11	-	498,40	0,89	-	0,015	-
28/12/2020	21	39000	11	11	11	498,30	0,81	0,019	0,015	0,018
26/01/2021	21	37000	11	11	11	498,20	0,83	0,021	0,015	0,021
30/01/2021	21	34500	11	11	11	498,20	0,86	0,017	0,013	0,016

Table 9:
Primary eclipses times for the observed eclipses.

Binary star system	Observation night	Filter	HJD_{min}
2MASS J01074282+4845188	01-11-2020	R	2459155.47614 ± 0.00022
		I	2459155.47614 ± 0.00030
	02-11-2020	R	2459156.44411 ± 0.00027
		I	2459156.44415 ± 0.00045
	03-11-2020	R	2459157.41162 ± 0.00012
		I	2459157.41202 ± 0.00020
ASAS J052919-1617.3	01-11-2020	V	2459155.64506 ± 0.00013
		R	2459155.64319 ± 0.00019
		I	2459155.64326 ± 0.00013
	03-11-2020	V	2459157.62726 ± 0.00017
		R	2459157.62715 ± 0.00032
		I	2459157.62722 ± 0.00035
	28-12-2020	V	2459212.47704 ± 0.00014
		R	2459212.47618 ± 0.00018
		I	2459212.47654 ± 0.00022